

# **Energetics of Lithium-Ion Battery Failure during Use and Thermal Abuse**

by

William Calcagno

A Thesis

Submitted to the Faculty of the

WORCESTER POLYTECHNIC INSTITUTE

In partial fulfillment of the requirements for the

Degree of Master of Science

In

Fire Protection Engineering

By

---

April 2022

APPROVED:

---

Professor James L Urban

---

Professor Albert Simeoni

---

Professor Milosh Puchovsky

**Abstract:**

This research tested the impact of the usage condition of lithium-ion batteries on their thermal runaway properties during thermal abuse in a modified copper slug calorimeter. Two chemistries of cylindrical 18650 lithium-ion cells were used:  $\text{LiNiMnCoO}_2$  (NMC) and  $\text{LiNi}_x\text{Co}_y\text{Al}_{1-x-y}\text{O}_2$  (NCA). During each test,  $20 \pm 0.2$  watts were used to heat the cell. During each test, discharge was simulated by a series of resistors connected to the top and bottom electrical contacts of the battery. It was found that the average time to thermal runaway for NCA cells decreased as discharge current increased, while the average time to thermal runaway for NMC cells increased if discharge was present but did not increase continuously with increased discharge current. It was also found that the average mass loss for NMC cells decreased as discharge increased, a trend that did not repeat in the NCA cell tests. In addition, it was observed that the NMC cells lost charge faster than the NCA cells, which resulted in NMC cells undergoing thermal runaway during the high-discharge tests at a significantly higher temperature than every other test condition. The spark velocity and duration of thermal runaway trends were similar between both battery types; average and maximum spark velocities decreased as discharge current increased and duration of thermal runaway increased as discharge rate increased except for the high-discharge NMC battery tests. Copper slug calorimetry results also showed the total internal heat generation in NMC battery tests increased as discharge current increased until the high-discharge tests, at which point the total internal heat generation dropped. NCA battery tests showed almost the opposite trend, where total internal heat generation values decreased as discharge rate increased until the high-discharge test condition where they increased. Peak internal heat generation values showed the same general trend between battery types, where they decreased as discharge rate increased. These results suggest that while this test methodology can be generalized and applied to different battery chemistries, the impact of a lithium-ion battery's usage condition (i.e., discharge current) on its thermal runaway properties cannot be generalized between different chemistries and each new chemistry should be tested in the future.

## **Acknowledgements**

I would like to thank my thesis advisor Dr. James Urban of Worcester Polytechnic Institute. Professor Urban was always available when I needed guidance and support for this research whether it was a question about the data or the writing of my thesis. If I had a question, he was always available to guide me to a resolution. He steered me in the right the direction whenever he thought I needed it or whenever I asked.

I would also like to thank an expert who was involved in the development and analysis for this research project. Dr. Ahmad Osama Said. Without his professional guidance and friendship, and invaluable input, this research would not have been successfully conducted.

I would like to express my gratitude to Abhinandan Singh for the guidance, direction and support of using LabVIEW. This support enabled me to analyze the research data in a useful and helpful format.

I would also like to thank the FPE Lab Mangers, Raymond Ranellone and Frederick Brokaw, for their support in assisting with the development of the research test apparatus and allowing me to spend many hours in the lab space to conduct my research.

I would also like to acknowledge Mrs. Diane Poirier, Administrative Assistant at Worcester Polytechnic Institute, for her ongoing support to the Fire Protection Engineering students in the department. Her dedication to the Fire Protection Engineering department and its students has been invaluable. Without her support and encouragement, this research success would not have been possible.

This project would not have been possible without the support generously provided by a WPI TRIAD seed grant and a Student Research Grant from the Society of Fire Protection Engineers Foundation.

Finally, I must express my very profound gratitude to my parents for providing me with unfailing support and continuous encouragement throughout my academic career and through the process of researching and writing this thesis. This accomplishment would not have been possible without them. Thank you.

## Table of Contents

Abstract: .....	2
Acknowledgements .....	3
Introduction .....	6
Background and Significance: .....	6
Lithium Ion Battery (LIB) Operation .....	7
Specific Aims and Objectives .....	11
Experimental Apparatus and Methods .....	11
LIB Sample Description and Preparation .....	12
Copper Slug Calorimeter .....	13
Charging/Discharging circuit .....	14
Experimental Procedure: .....	15
Results & Discussion .....	17
Spark Velocity Analysis .....	32
Conclusions .....	36
Appendix A: Battery Test Data .....	40
Appendix B: Copper Slug Calorimetry Equations .....	43
References .....	44

## **Introduction**

### Background and Significance:

Lithium-ion batteries (LIBs) have become increasingly common in modern technology due to their high energy density. This high energy density, however, poses higher risks if the battery enters thermal runaway and initiates a fire. While the likelihood of a single lithium-ion battery entering thermal runaway is relatively small, the ubiquitous presence of these batteries in personal electronic devices, electric vehicles, and even grid-scale energy storage results in a significant number of fires. Furthermore these fires have been shown in some cases to happen often in locations that amplify the danger, such as airplanes<sup>1</sup>. Over 290 incidents “with smoke, fire, extreme heat or explosion” involving lithium metal and lithium-ion batteries were reported by the Federal Aviation Administration (FAA) in August 2020 alone<sup>1</sup>. The number of incidents on planes has been increasing over the years as well, due to the increased usage of lithium-ion batteries. However, this only accounts for lithium-ion battery incidents on planes and not for any other incidents, which may go un-reported/documented.

Being a relatively new technology, lithium-ion batteries are still being incorporated into relevant fire codes, regulations and standardized tests. Current regulations for lithium-ion batteries focus on production, safety checks and transport regulations<sup>2</sup>, with the first NFPA code dedicated to the installation of energy storage systems, NFPA 855, released in 2020. Changes are still being made to existing codes to account for the increasing prevalence of lithium-ion batteries in modern-day technology (e.g., electronic devices, electric vehicles, etc.), with recommendations being released as they continue to be developed<sup>3</sup>. Differences in behavior between different battery chemistries when used in thermal abuse conditions remain unexplored and can potentially pose design risks when designing systems involving lithium-ion batteries. The scope of these changes

can range from airplanes to parking garages as LIBs become more integrated into the built environment.

### Lithium Ion Battery (LIB) Operation

Unlike typical solid fuels encountered in fire research (e.g., polymers, composites, etc.), LIBs are composed of several components which operate together as an energy storage device and may also have various types of safety features, such as safety venting, which may control the thermal behavior during fire conditions. The key components of Lithium-ion batteries are typically an anode, separator, cathode, and electrolyte, and are shown in Figure 1. The cathode material contains the transition metal oxide and takes in electrons from the anode<sup>4</sup> during discharging. Anodes are often graphite or  $\text{Li}_4\text{Ti}_5\text{O}_{12}$  (LTO) and the electrolyte in a lithium-ion battery is an organic solvent with lithium-based salts dissolved within. The separator prevents anything other than lithium ions from passing between the cathode side of the battery and the anode side. When a lithium-ion battery is being charged, lithium ions separate from the cathode and move to the anode, and the reverse happens when the battery is discharged.  $\text{LiNi}_x\text{Co}_y\text{Al}_{1-x-y}\text{O}_2$  (NCA) and  $\text{LiNiMnCoO}_2$  (NMC) lithium-ion batteries were used for these tests as they are two of the higher energy density chemistries for lithium-ion cells and thus would have some of the most energetic reactions. Because of their high energy density, they are also commonly used in devices including electric vehicles.

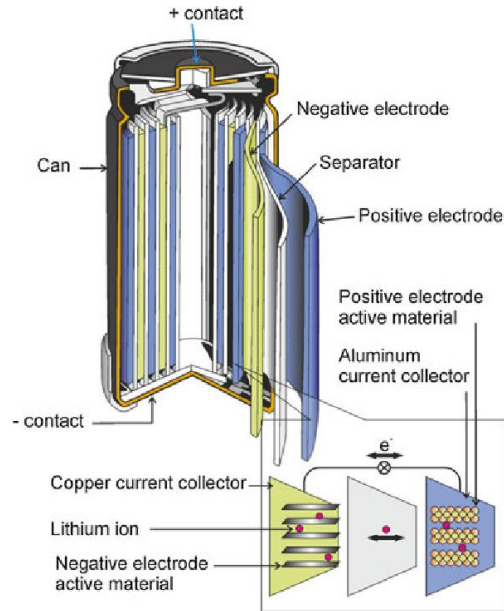


**Figure 1:** The internal schematic of a cylindrical lithium-ion battery<sup>5</sup>

Lithium-ion batteries come in several different formats, the most common of which are cylindrical, prismatic and pouch<sup>6</sup>. Cylindrical cells are the most common of the three, with all of the battery's components rolled and fitted inside a rigid cylindrical body (see Figure 1). Prismatic cells use a rigid rectangular body but are constructed in a similar manner to cylindrical cells, with the internal components folded to fit as much as possible into the space. Pouch cells are the only one of the three most common forms that do not have a rigid body, nor are their internal components rolled or folded; they are instead stacked to fill their pouch. While these batteries operate using similar components and battery chemistries, the behavior and safety features vary between different formats and chemistries.

For cylindrical format batteries, safety venting is one of a lithium-ion battery's most important safety features during thermal abuse<sup>7</sup>. As the battery heats up, its internal pressure increases. Safety venting occurs when this internal pressure exceeds the limit of a "vent disc," also known as a current interruption disc (CID)<sup>8</sup>, which is designed to fail before the separator between the anode

and cathode can start to degrade. The vent disc in cylindrical cells is a component of the battery's discharge circuit, so when the vent disc fails it also cuts off the internal connection in the battery, preventing further discharge. Another important safety component is the positive terminal coefficient switch (PTC). The PTC is next to the vent disc within a battery and increases the battery's internal resistance as its temperature increases<sup>9</sup>.

Thermal runaway in batteries can be started through a combination of manufacturing defects and/or external abuse. The variety of LIBs and their applications results in a wide variety of potential abuse conditions, but many cases can be categorized as mechanical abuse (e.g., penetration of battery casing, compression, etc.), thermal abuse (e.g., exposure to fire or heat source, lack of thermal management), or electrical abuse (e.g., short circuiting or improper use/installation). To better understand the danger posed by these types of abuse, experiments have been developed to recreate these types of abuse in a controlled, repeatable manner. Penetration testing, one of the most common types of mechanical abuse testing<sup>10</sup>, functions by remotely pushing a nail into a battery to pierce the separator in the battery. Testing has shown that the penetration velocity into a lithium-ion battery has a greater impact on thermal runaway characteristics than the location of penetration<sup>11</sup>. Thermal abuse triggers thermal runaway by degrading the separator in the battery. When the separator breaks, whether through degradation or physical damage, it causes a short circuit within the battery, one of the most common forms of electrical abuse<sup>12</sup>. The second law of thermodynamics tells us energy transfer generates heat. This heat leads to further weakening of the separator, which increases the scale of the short circuit inside the battery leading to an accelerating runaway reaction.

There have also been studies examining the energetics of thermal runaway and what factors influence it. Studies have examined how lithium ion batteries behave in different environmental

conditions which impact thermal runaway and battery fires such as low atmospheric pressure<sup>13</sup> and lower oxygen concentration<sup>14</sup>. There has also been research examining how the LIB chemistry, components, and state of charge impact the onset temperature and peak temperature of thermal runaway<sup>15</sup>. Similar studies have also examined the gases produced during thermal runaway<sup>16</sup>.

Despite this research, very little research has been done on how the state of use impacts thermal runaway. A recent study examined how thermal abuse during charging impacts battery heating and thermal runaway<sup>17</sup>. It was found through this study that charging a lithium-ion battery during thermal abuse causes thermal runaway to occur prematurely. This result begs the question of “if charging has an impact on thermal runaway times, what about discharging?” Another study researched a behavior of failing LIB packs, “Current dumping,” where the current through a lithium-ion battery cell increases when another cell in the circuit fails<sup>18</sup>. The researchers in this study found that as the current increases, so does the failure propagation rate, which supports the idea that the time it takes a lithium-ion battery to undergo thermal runaway decreases if its current usage requires a higher discharge rate. This failure mode highlights the need to understand the role of electrical use, how it compares to electrical abuse and also how aspects of the LIB, such as state of charge, may change during the failure event rather than just assuming a constant value.

Determining how the usage of a lithium-ion battery impacts the onset of thermal runaway could change how future lithium-ion battery testing is performed. If the results show that one state of use results in a quicker onset of thermal runaway than other states of usage, it may be necessary to reexamine current methods of determining the safety of lithium-ion batteries. This project aims to answer the question of how a lithium-ion battery’s state of use impacts its characteristics of thermal runaway.

## Specific Aims and Objectives

The major aim of this project is to determine the impact usage (i.e. discharging while powering electronics) has on the tendency for a Lithium-ion battery to initiate thermal runaway and the subsequent heat release while simultaneously experiencing thermal abuse. During discharging, the state of charge of the battery will decrease, changing stored chemical energy (i.e. potential to release energy) into electrical power carried out of the battery while dissipating heat in the battery. In this study, two Lithium-ion battery chemistries will be used: LiNiMnCoO<sub>2</sub> (NMC) and LiNi<sub>x</sub>Co<sub>y</sub>Al<sub>1-x-y</sub>O<sub>2</sub> (NCA) batteries<sup>15</sup> as they are two of the most energy-dense lithium-ion battery chemistries readily available and should have more energetic reactions than other chemistries. These battery chemistries are often seen in battery packs of common electrical vehicles with the same LIB format (cylindrical cell). The conditions under which the batteries undergo thermal runaway will be examined through experiments exposing batteries to a prescribed heating rate while the LIB undergoes different discharge currents.

The results of this work will give engineers a better understanding of how battery usage during thermal abuse impacts thermal runaway properties and illustrate the worst-case scenario for each lithium-ion battery chemistry. This information could lead to better thermal management systems in batteries and better fire safety regulations and standards.

## **Experimental Apparatus and Methods**

Previous research has used several other forms of calorimetry<sup>19</sup>, such as accelerating rate calorimetry (ARC), but copper slug calorimetry<sup>4</sup> was used in these experiments as it measures the battery's heat directly. Additional forms of calorimetry, such as oxygen consumption calorimetry, were not used, resulting in the heat release of expelled gases not being quantified. The high

velocity of the ejected gases would have made it difficult to collect all of the gases to get an accurate result. The copper slug calorimeter is detailed below.

LIB Sample Description and Preparation



**Figure 2:** Pairs of NMC (left pair) and NCA (right pair) lithium-ion batteries. Within each pair, untested battery cells are on the left and tested battery cells on the right.

The batteries used in this study were cylindrical 18650 format, which is named for the nominal dimensions of the batteries, 18 mm diameter and 65 mm height. The battery chemistries were NCA and NMC (shown in Figure 2) from two different manufacturers (see Table 1). Before each battery was tested, their plastic wrappings were removed, and they were cycled from full charge to empty and back again twice before being charged to full capacity with the battery charging patterns recorded for later analysis. If the batteries were tested on a different day than when they were charged, the batteries were charged back to full before testing.

**Table 1:** Battery Chemistry, manufacturer, nominal capacity, nominal voltage and maximum continuous discharge

Battery Model	Battery Chemistry	Manufacturer	Nominal Capacity (mAh)	Nominal Voltage (V)	Maximum Safe Continuous Discharge Current (A)
LG-MH1-18650-INR <sup>20</sup>	NMC	LG Chem	3,200	3.67	10
NCR 18650A <sup>21</sup>	NCA	Panasonic	3,070	3.6	6.2

### Copper Slug Calorimeter

At the start of each test, the charged battery was mounted in the thick-walled copper tube of the copper slug calorimeter (See Figs. 3 & 4). The copper tube is 65 mm long, with an outer diameter of 25.4 mm and inner diameter of 18 mm. Two small diameter holes were drilled in the wall of the copper tube to place a sheathed K-type thermocouple (OMEGA TJ36-CAXL-020G-12) to monitor the temperature of the copper slug which is assumed to be very close to the temperature of battery. Superwool Insulation Board 85 plus<sup>22</sup> was used to minimize heat losses to the outside. Measurements from the thermocouple were data-logged using LabView at a rate of 5Hz.



**Figure 3:** The calibration set-up of the experimental test apparatus

### Charging/Discharging circuit

A circuit was formed by connecting the battery terminals to a resistive load or placed in an “open circuit” configuration. In each test, the LIB was subjected to different discharge currents below the maximum safe discharge current designated by the manufacturer (listed in Table 1), or what would normally be considered “safe” operation if the LIB were undamaged and under appropriate thermal regulation. The different discharge currents of the batteries were obtained by changing the resistance in the discharge circuit (see Figure 4). In open circuit tests (no discharge), the copper electrical contacts of the discharge circuit are present even when not discharging or charging to ensure the batteries are tested under the same conditions. The battery is placed in a copper cylinder wrapped in electrically insulated nichrome wire connected to a heater, and the bottom electrical contact wire taped to the bottom of the battery with the same tape used to wrap the cylinder. The top electrical contact is lowered into place after the cylinder is placed inside the test assembly and strapped down. Changes to the electrical contacts between different test conditions are kept minimal; different resistors are attached by cutting the wires connected to the resistors and soldering a new resistor in place. The increase in resistance from the solder is insignificant<sup>23</sup>. The nichrome heater is powered by an external power source.

Four types of battery use conditions were tested in this project: a control test and high, medium and low discharge tests. During the control tests, the batteries were neither charging nor discharging, with the electrical contacts left unconnected or were electrically insulated. During the discharging tests, the batteries were connected to a resistor, far enough away from the test set-up that any heat generated by the resistor would not impact the battery. The resistances were selected to simulate safe discharge rates below the maximum safe discharge rate provided by the manufacturer to simulate normal operation if the elevated heating were not present. High-

discharge tests used a resistance of 0.8-ohms, medium-discharge used a resistance of 1.4-ohms and low-discharge used a resistance of 2.7-ohms. Resistors were constructed of several larger resistors soldered in parallel on a bread board in order to create the desired resistance ( $\pm 0.2$  ohms).

Cold tests, where the batteries are discharging at the High rate but are not undergoing external heating, were performed to determine their discharge heating rates. Tests were performed over a ten-minute period, with the batteries being charged immediately afterward to determine the amount of charge lost during those ten minutes. The NCA battery's temperature raised by 39.9 °C and it lost 944 milli-Amp-hours (mAh), while the NMC battery's temperature raised by 44.5 °C and it lost 2292 mAh.

#### Experimental Procedure:

When the batteries were tested under the fume hood, the testing apparatus was first prepared by checking that the copper cylinder was still wrapped in electrically insulated nichrome wire and the copper pieces used for charging/discharging the battery were free of corrosion. The battery was then weighed before being put into the copper cylinder. The cylinder was then placed in the test apparatus and the test apparatus was closed before being placed on the mass balance. The top electrical contact was then moved into contact the battery. The power supply was then plugged in and calibrated to ensure the heating element was set to twenty watts before two thermocouples were placed in the cylinder to monitor the battery's temperature. A camera (Sony DSC-RX10M4) was placed at a safe distance to observe and record the tests. All observers then moved to a safe distance away or behind cover as the power supply and data recording were started.

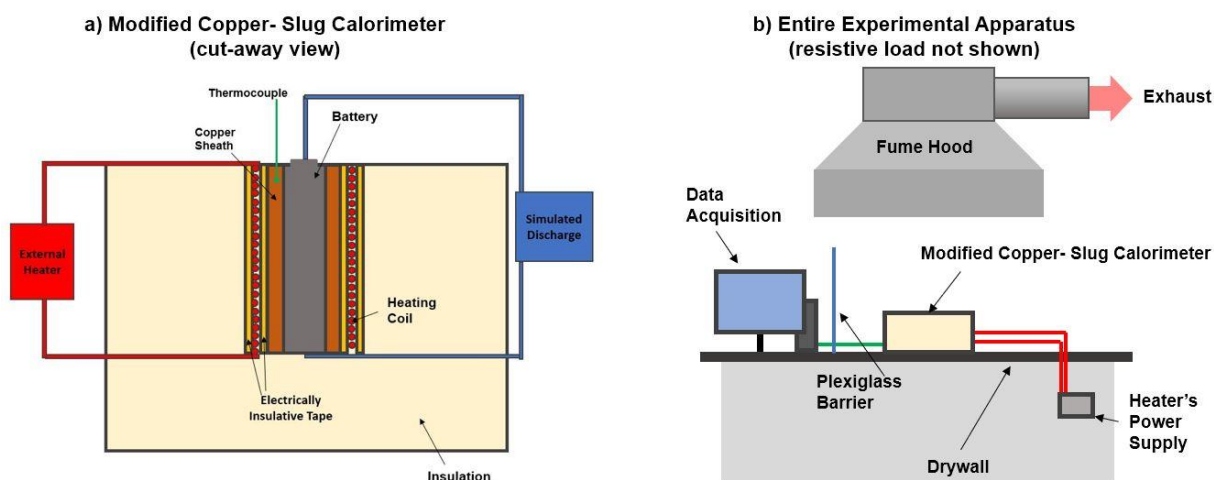


**Figure 4:** a) Detailed schematic of test rig and b) entire experimental set-up. (not to scale)

**Table 2:** Number of tests performed per test condition.

	Control	Low Discharge	Medium Discharge	High Discharge
NMC Batteries	5	5	5	5
NCA Batteries	5	5	5	5
Resistance (Ohms)	0	2.7	1.4	0.8

For each experiment, the time-dependent data was analyzed. The thermal onset time and temperature will be determined and other time dependent measurements (state of charge, current) at the onset of thermal runaway and immediately following. A thermal analysis of the battery and metal sheath will be performed with the thermocouple and heater power data similar to work by others<sup>24</sup>. This will elucidate the interplay between the heating of the battery and the reduction of the state of charge during the experiment.

The data collected during these tests can be used in several different ways. Some of these uses include determining a battery's susceptibility to thermal runaway, modelling lithium-ion battery

failure and cascading lithium-ion battery failure, and determining criteria for battery management systems.

## **Results & Discussion**

Much of the data analysis revolves around the temperature of the cell (assumed to be in thermal equilibrium with the surrounding copper tube) during the tests. Figure 5 shows the transient temperature of the cell during an example test (NCA cell without discharge) with important events labeled (safety venting, thermal runaway, and duration of burning) and Figures 6 & 7 show safety venting, spark production, and a jet flame). After each test started, the primary sources of heating were the external heater and discharge heating; there was no internal heating at this time.

When safety venting occurs, the vent disk bursts, releasing a puff of gas. This puff of gas carries some of the battery's energy with it, causing a momentary drop in temperature and small drop in mass. Safety venting also cuts off the connection between the positive and negative electrodes within the battery, preventing discharge and discharge heating

The external heater remained on after safety venting, causing the temperature of the battery to continue climbing. Eventually, the battery's temperature rose enough that the separator between the anode and cathode started to degrade, causing internal discharge and internal heating. This internal heating continued to increase until thermal runaway occurred, at which point the external heater was turned off.

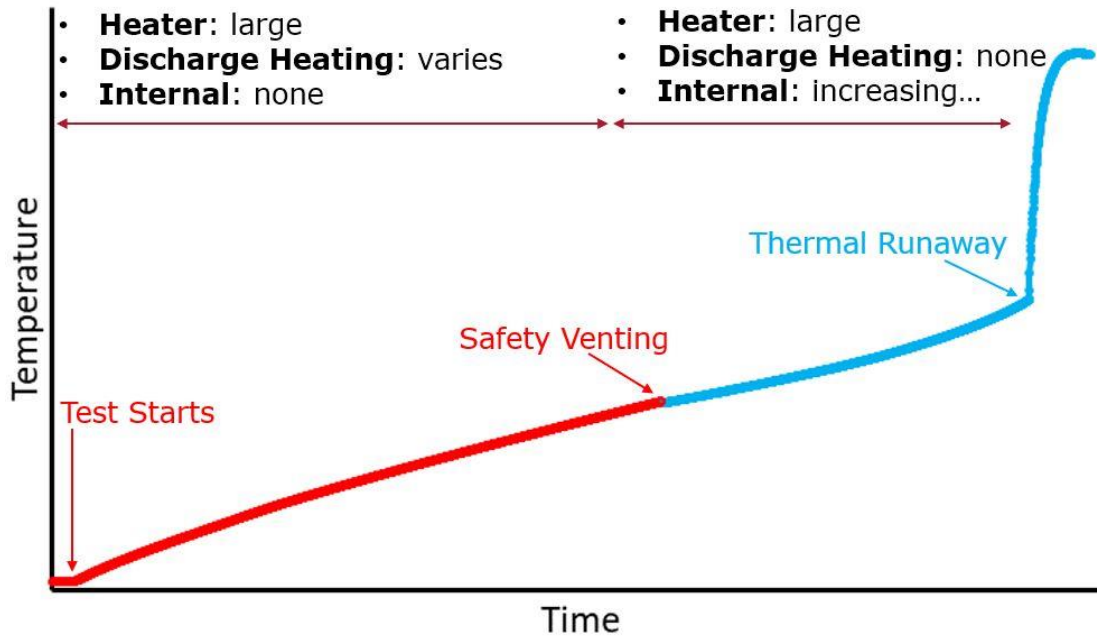


**Figure 5:** Battery heating from safety venting to thermal runaway.



**Figure 6:** The puff of gas released during safety venting

When thermal runaway occurred, a stream of sparks emerged from most of the batteries, followed by a flame rising from the top of the battery. The positive contact on the battery remained in most tests but was broken off by the force of thermal runaway during some of the tests.



**Figure 7:** Thermal runaway spark streams (left) and flames (right).

The timing and intensity of these events depended on the test conditions (discharge current and battery chemistry). Figure 8 shows representative battery heating curves for NCA and NMC batteries.

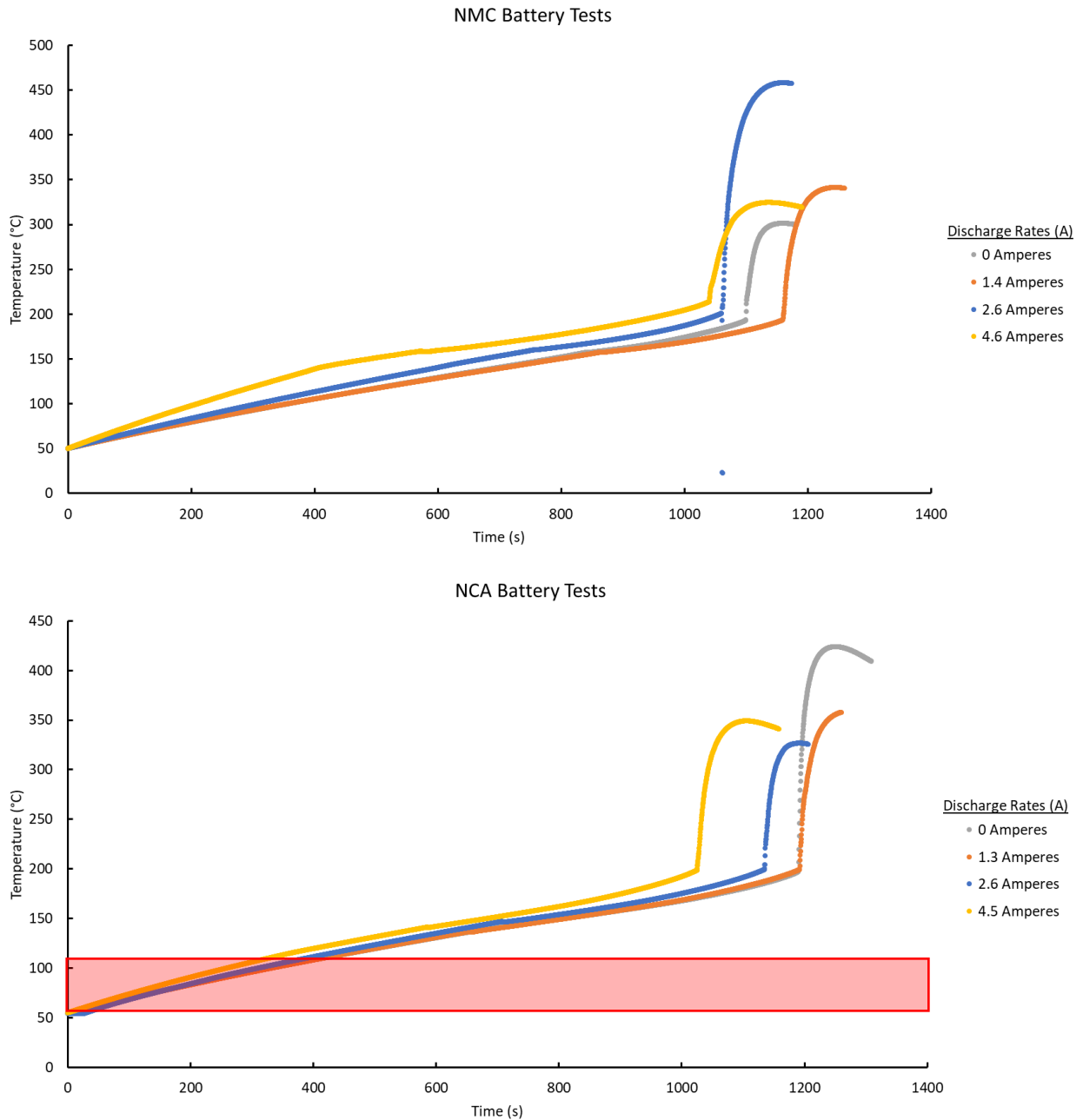


**Figure 8:** Representative tests of NMC (Top) and NCA (Bottom) batteries at different discharge currents below the discharge current listed by the manufacturer. The red box is the temperature range previous research has determined to be the start of self-heating in NCA batteries.

Previous research<sup>15</sup> has found that separator degradation begins at temperatures less than 100°C and that separator breakdown in NCA batteries peaks around 140°C, around when safety venting was observed to occur on average during the tests performed in this paper. Temperatures

immediately after safety venting were observed to be lower than pre-safety venting, and internal heat generation (discussed later in the paper) dropped dramatically during safety venting, leading to the conclusion that separator breakdown is an endothermic process. The red box in the bottom graph in Figure 8 is the temperature range (51-103°C) in which the self-heating in NCA batteries begins<sup>15</sup>. NMC lithium-ion batteries were not one of the chemistries studied in the referenced research and so no equivalent box has been included in the NMC representative test graph.

During testing, thermal runaway was observed to occur at a consistent temperature range, typically varying between 193°C and 200°C, with the exception of the high discharge current NMC battery tests. The high discharge NMC tests had an average thermal runaway temperature of  $218.8 \pm 2.35^\circ\text{C}$ . These values are plotted in Figure 9.

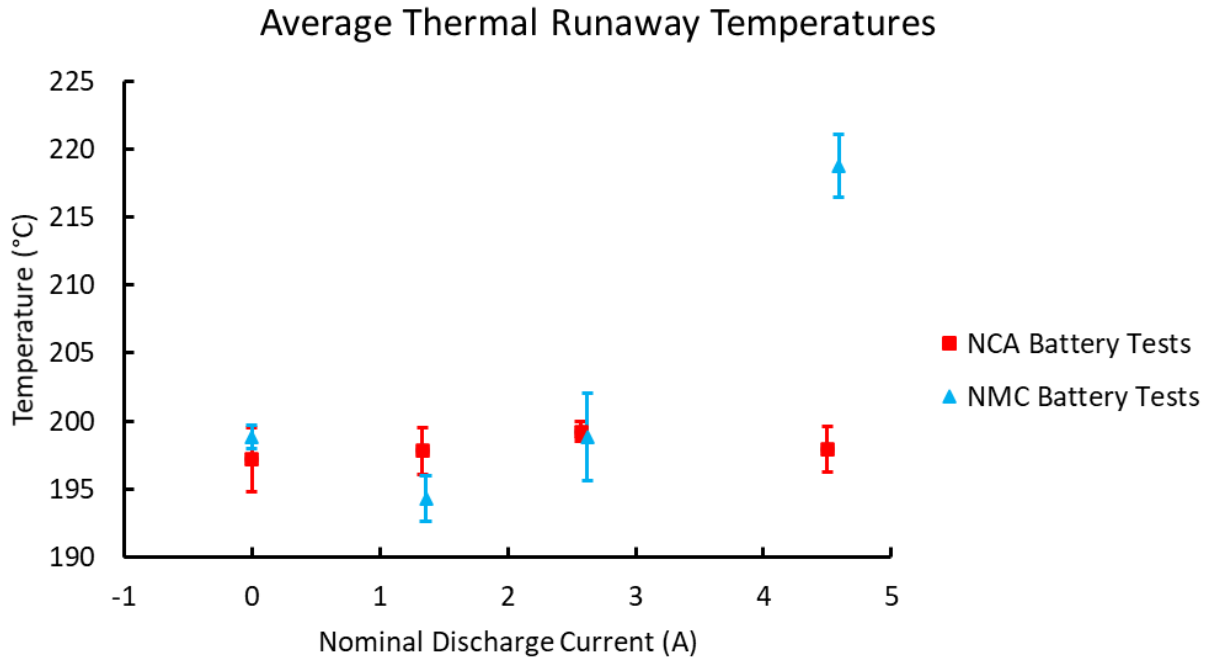


**Figure 9:** Average thermal runaway temperatures for each test condition and battery type. Error bars show a 95% confidence interval.

The average safety venting temperatures for each test condition and battery type are plotted in Figure 10. Both the NCA batteries and NMC batteries show the same trend: the average safety venting temperature increases slightly with increased discharge currents, with the NCM battery tests consistently undergoing safety venting 12-15°C higher than the NCA batteries.

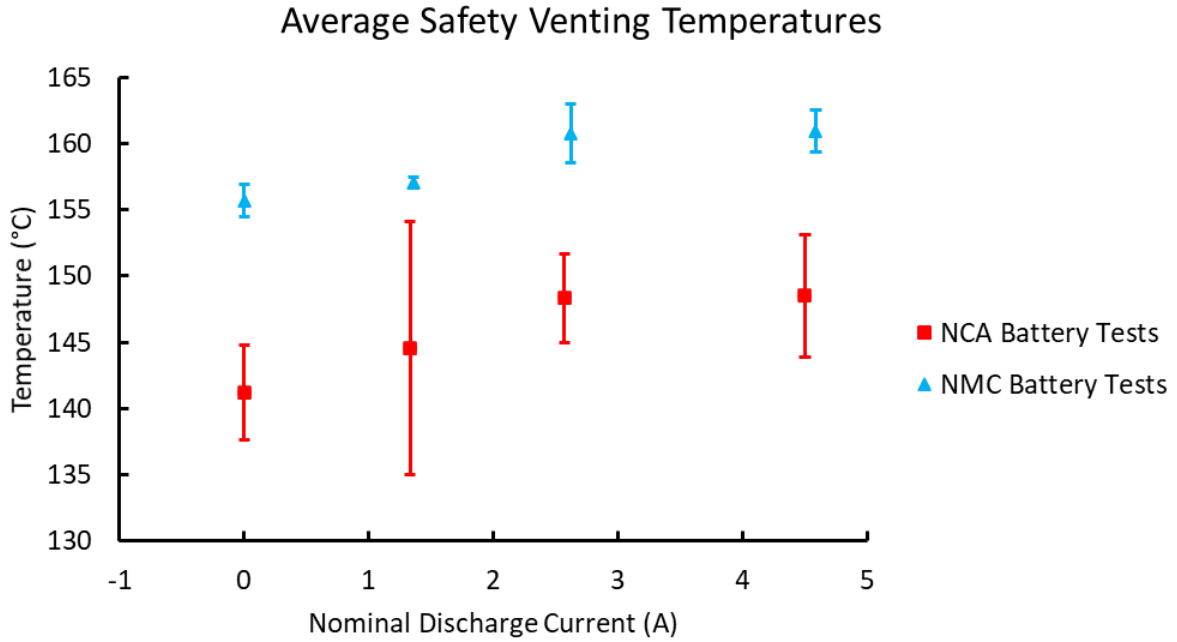


**Figure 10:** Average safety venting temperatures for each test condition and battery type. Error bars show a 95% confidence interval.

The average mass losses for each test condition and battery type are plotted in Figure 11. Percentages were used rather than grams as the initial mass for each cell was approximately 44 grams, so any mass losses initially appear small. There is no clear mass loss trend in the NCA battery tests, but there is a clear trend in the NCM average mass loss data. A trendline has been included to show this clear trend in the average NMC mass loss, where the average mass loss decreases as discharge rate increases.

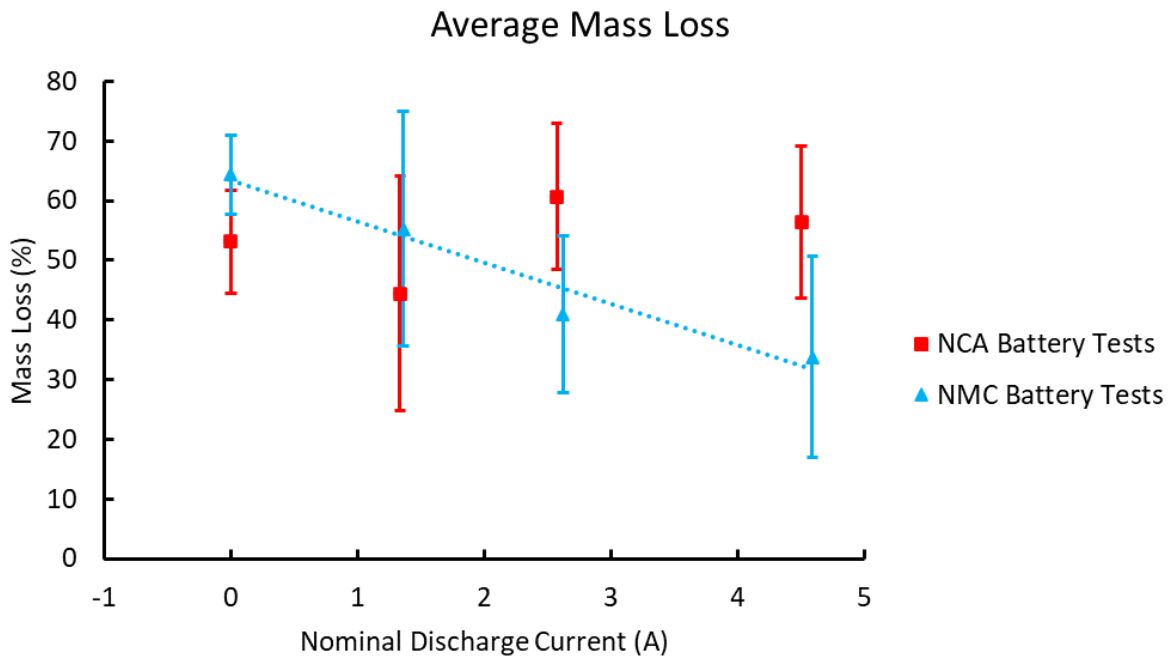


**Figure 11:** Average mass loss, in percent, for each test condition and battery type. Error bars show a 95% confidence interval.

The average time from 55°C to thermal runaway for each test condition and battery type are plotted in Figure 12. A baseline temperature of 55°C was chosen to have the same starting point for data analysis, as the actual starting conditions varied day by day due to weather and other uncontrollable variables. A trendline was included to show the clear trend in the NCA battery tests, with the time to thermal runaway decreasing as the discharge current increases. Almost the opposite trend is seen with the NCM battery tests, as the time to thermal runaway increases or stays the same as discharge rate increases.

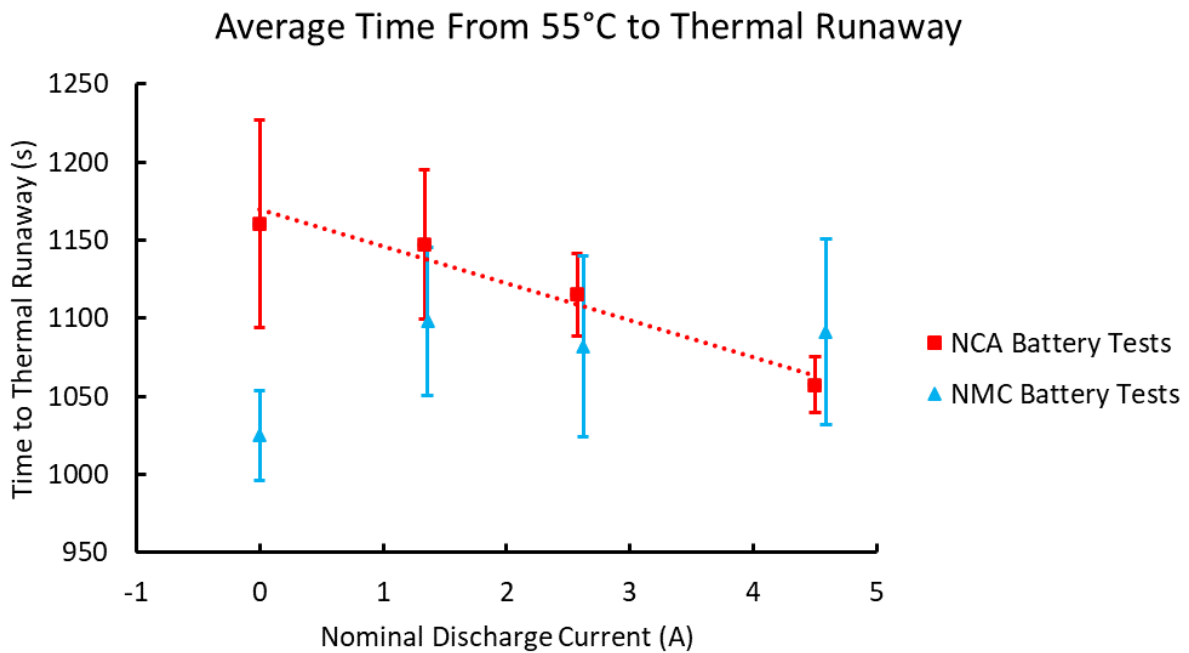


**Figure 12:** Average time to thermal runaway for each test condition and battery type. Error bars show a 95% confidence interval.

The average times to safety venting for each battery chemistry and test condition are plotted in Figure 13. Both battery chemistries share one pattern: the time to safety venting increases from no discharge to low discharge, then decreases as discharge increases. This decrease is more severe in the NMC tests, where the average time to safety venting for high-discharge tests is significantly lower than any other test condition.

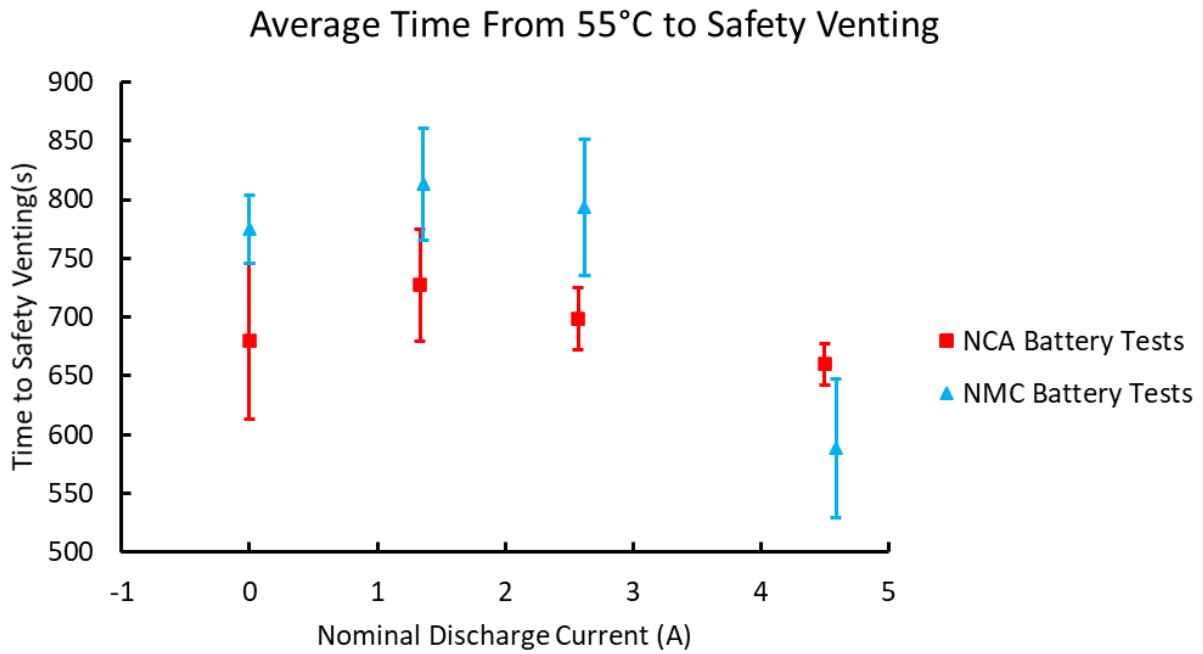


**Figure 13:** Average time to safety venting for each battery type and test condition. Error bars show a 95% confidence interval.

The average maximum temperature of the copper sheath post thermal runaway for each test condition and battery type is plotted in Figure 14. This maximum temperature appears to increase as discharge rate increases for the NMC battery tests and decrease for the NCA battery tests. It is difficult to confirm these trends, however, as the 95% confidence intervals for each test condition overlap.

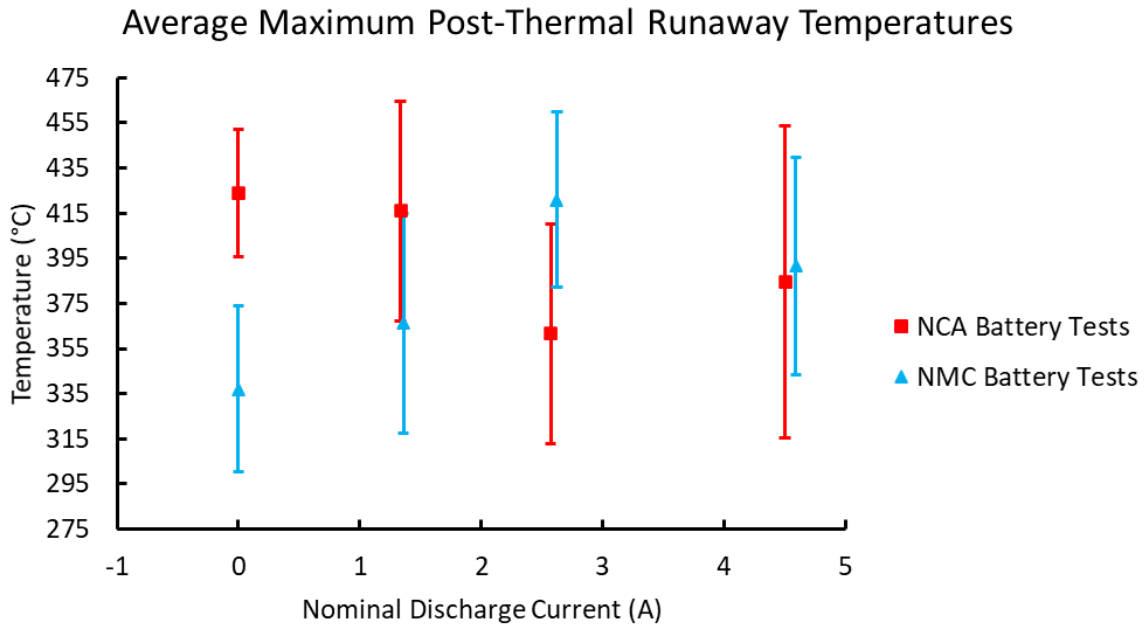


**Figure 14:** Average maximum recorded test temperature post thermal runaway for each test condition and battery type. Error bars show a 95% confidence interval.

The average duration of thermal runaway was calculated through

$$D = n/r, \quad (2)$$

where  $D$  is the duration of thermal runaway,  $n$  is the number of frames in a test video from the onset of sparks until spark release stops and  $r$  is the frame rate of the video. These duration values were then averaged by battery type and test condition and plotted in Figure 15. There is a clear trend in the NCA tests, with the duration of thermal runaway increasing as nominal discharge current increases, although this increase appears to level out from medium discharge to high discharge. A different trend is present in the NMC battery tests; the average thermal runaway duration appears to be level from no discharge to low discharge, increased as nominal discharge increases to medium, then drops to the lowest average duration of all tests in high discharge tests. This latter drop is a result of the lower state of charge of the NMC battery during thermal runaway during this test condition.

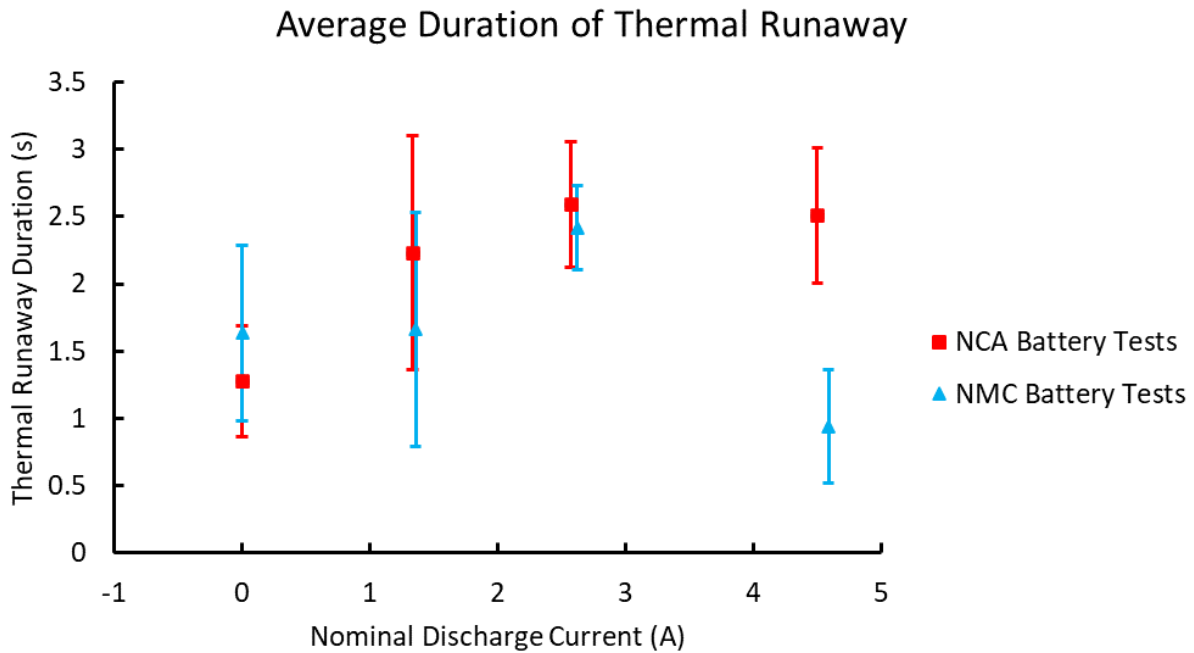


**Figure 15:** Average duration of thermal runaway for each battery and test condition based on visual observation. Error bars show a 95% confidence interval.

Copper slug calorimetry was performed using the temperature data collected throughout the tests and the mass of each battery collected before and after each test. The results of this is total internal heat generation ( $\Sigma$ ) for each battery tested, these values are plotted in Figure 16 and calculated through

$$\Sigma = \int_{t_{T=55^{\circ}C}}^{t_{T=T_{peak}}} (IHG)dt \quad (2)$$

where IHG is the internal heat generation in watts and the integral period from 55°C to the peak temperature post-thermal runaway. A complete sample calculation is given in Appendix B. The calorimetry shows that the internal heat generation of the NMC batteries increased as discharge rate increased, with the exception of the high-discharge test condition. This is likely due to the lower state of charge of the battery during thermal runaway in the high-discharge test condition. The NCA battery internal heat generation had a different trend, where the average energy produced decreased as discharge rate increased with the exception of the high-discharge test condition.

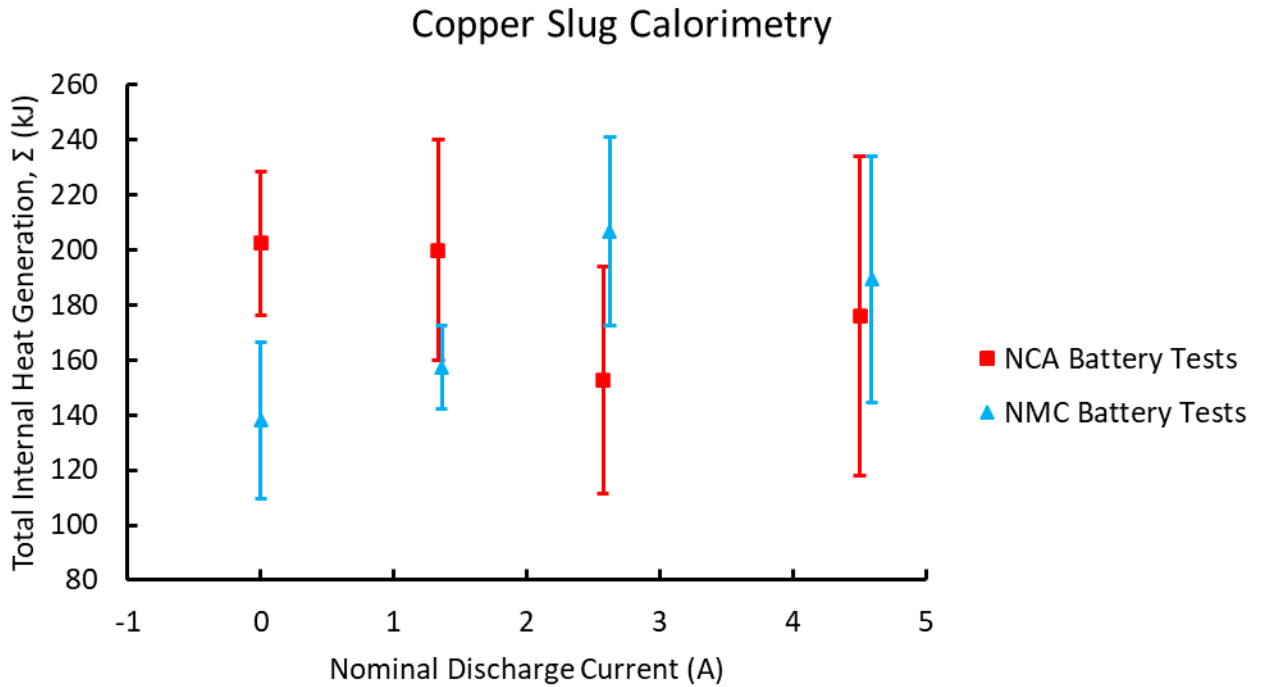


**Figure 16:** The total internal heat generation measured with copper slug calorimetry. Error bars show a 95% confidence interval.

There was one other unusual aspect about the NMC battery internal heat generation. A side-by-side comparison of NMC battery internal heat generation in medium and high discharge test conditions reveals that the battery during the high discharge test condition was producing almost 20 watts additional heating from the start of the test until the battery’s state of charge fell sufficiently. A similar pattern is observed when comparing internal heat generation in NCA batteries between medium and high discharge, although the initial heating is less than half that of the NMC internal heat generation. The blue arrows of Figures 17 and 18 indicate when safety venting occurs and the large temperature spike at the end of each graph is thermal runaway.

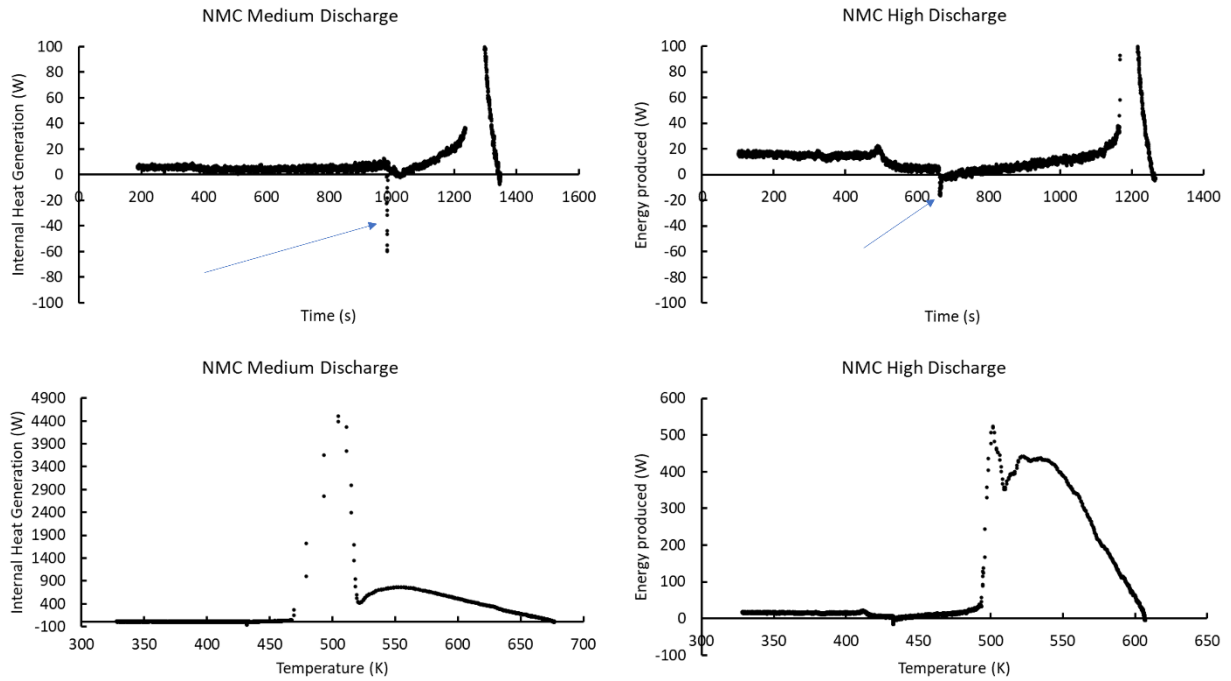


**Figure 17:** A comparison of medium (left) and high discharge (right) test condition calorimetric data of NMC batteries. Internal heat generation vs time graphs are plotted on top and internal heat generation vs temperature are plotted on the bottom.

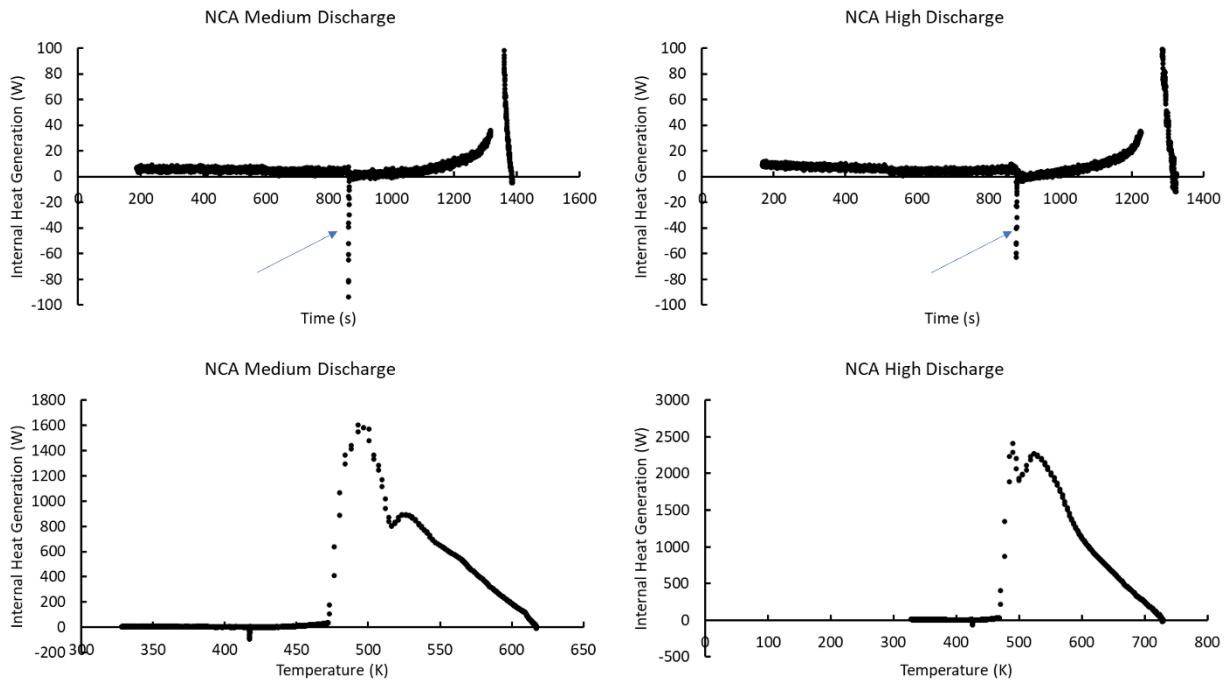


**Figure 18:** A comparison of medium (left) and high discharge (right) test condition calorimetric data of NCA batteries. Internal heat generation vs time graphs are plotted on top and internal heat generation vs temperature are plotted on the bottom.

Peak internal heat generation patterns also varied with test conditions. Both NCA and NMC showed a similar pattern, with peak internal heat generation values decreasing as discharge rate increased. Some of the discharge tests had significantly higher peak internal heat generation values though, likely due to variations in battery manufacture. Figure 19 shows these outliers as well as a zoomed in graph to observe the general trend without being influenced by outlying values.

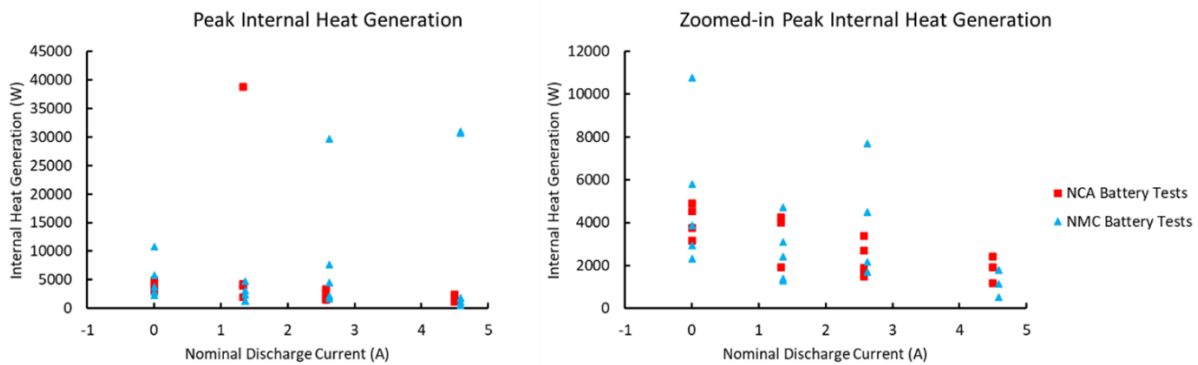


**Figure 19:** Peak internal heat generation values for all tests performed in this project. All data points are shown on the left, with a zoomed-in focus on the right to show patterns.

All of these values are tabled in Appendix A; Table A1 for NCA battery tests and Table A2 for NMC battery tests.

### Spark Velocity Analysis

The average velocity of the sparks from thermal runaway were also measured to determine how the test condition impacted this aspect of thermal runaway. In video recordings of each test, the sparks released during thermal runaway showed up as motion-blurred streaks. The length of these streaks was determined using a custom Python program to first find the length of the streak image (pixel-length) and then scale that measurement to an actual length scale, using a spatial calibration created before each test. The velocity of each spark was calculated through

$$V = L/\tau \quad (3)$$

where  $V$  is the velocity of the spark,  $L$  is the length of the spark's streak and  $\tau$  is the exposure of the frame in the video. These velocities were plotted for each test condition and battery type, with NCA battery tests plotted in Figure 18 and NMC battery tests plotted in Figure 19. The maximum, median and minimum spark velocities were also determined and listed in Tables 3 (for NCA batteries) and 4 (for NMC batteries).

Many sparks could not be used for determining spark velocities due to going off-screen or being in a cluster of other sparks such that the start or end point of an individual spark-streak in the cluster could not be determined. Additionally, the camera is only able to record a 2D projection of the spark's motion – as a result, sparks were sampled in regions of the image where the sparks motion would be primarily in the same plane as the image.

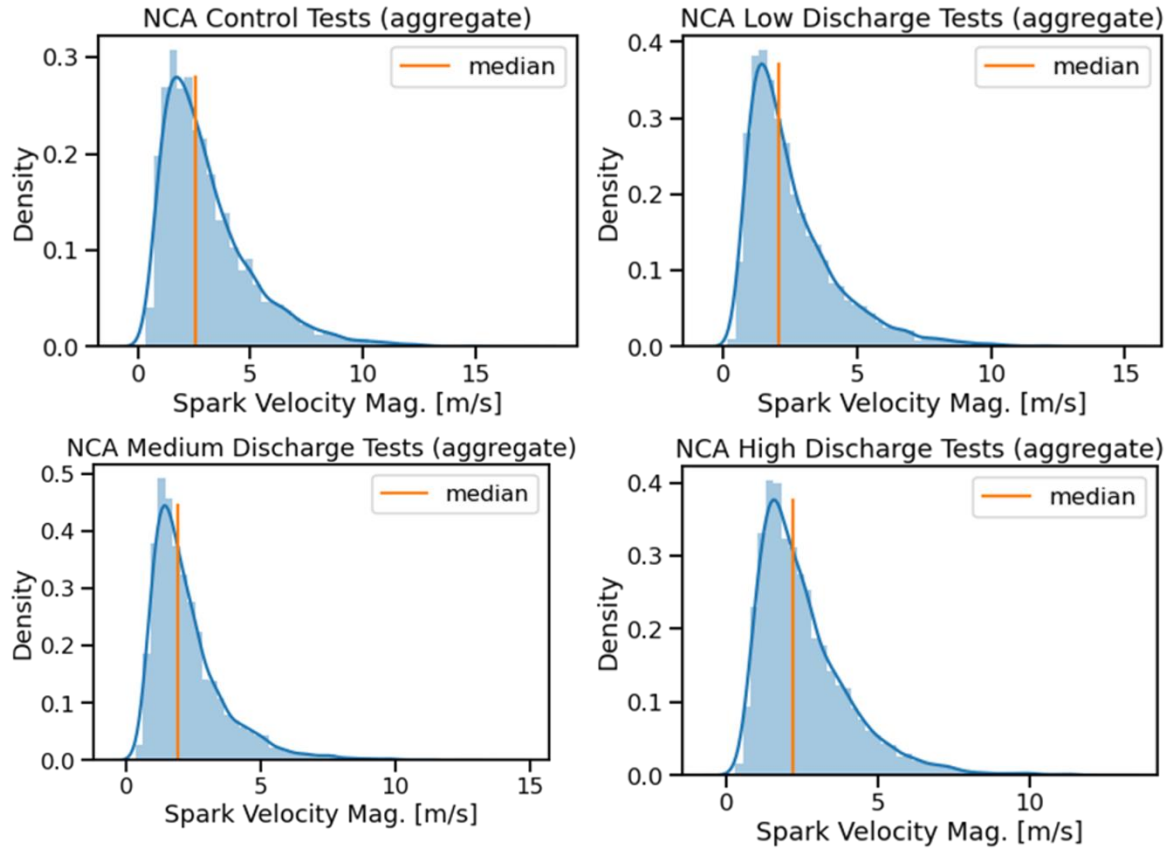


**Figure 20:** Aggregate spark velocity graphs for all NCA battery tests.

**Table 3:** Spark velocity values for NCA battery tests

	Control Tests	Low Discharge Tests	Medium Discharge Tests	High Discharge Tests
Maximum velocity (m/s)	17.39	14.68	14.15	12.71
Mean Velocity (m/s)	3.11	2.59	2.3	2.59
Median Velocity (m/s)	2.57	2.08	1.9	2.21
Minimum Velocity (m/s)	0.37	0.16	0.33	0.04

The spark velocities had the highest median and greatest variance during the control tests and were consistently lower during the other discharge tests. The median velocity does not appear to decrease continuously as discharge rates increase but appears to decrease if discharge is present.

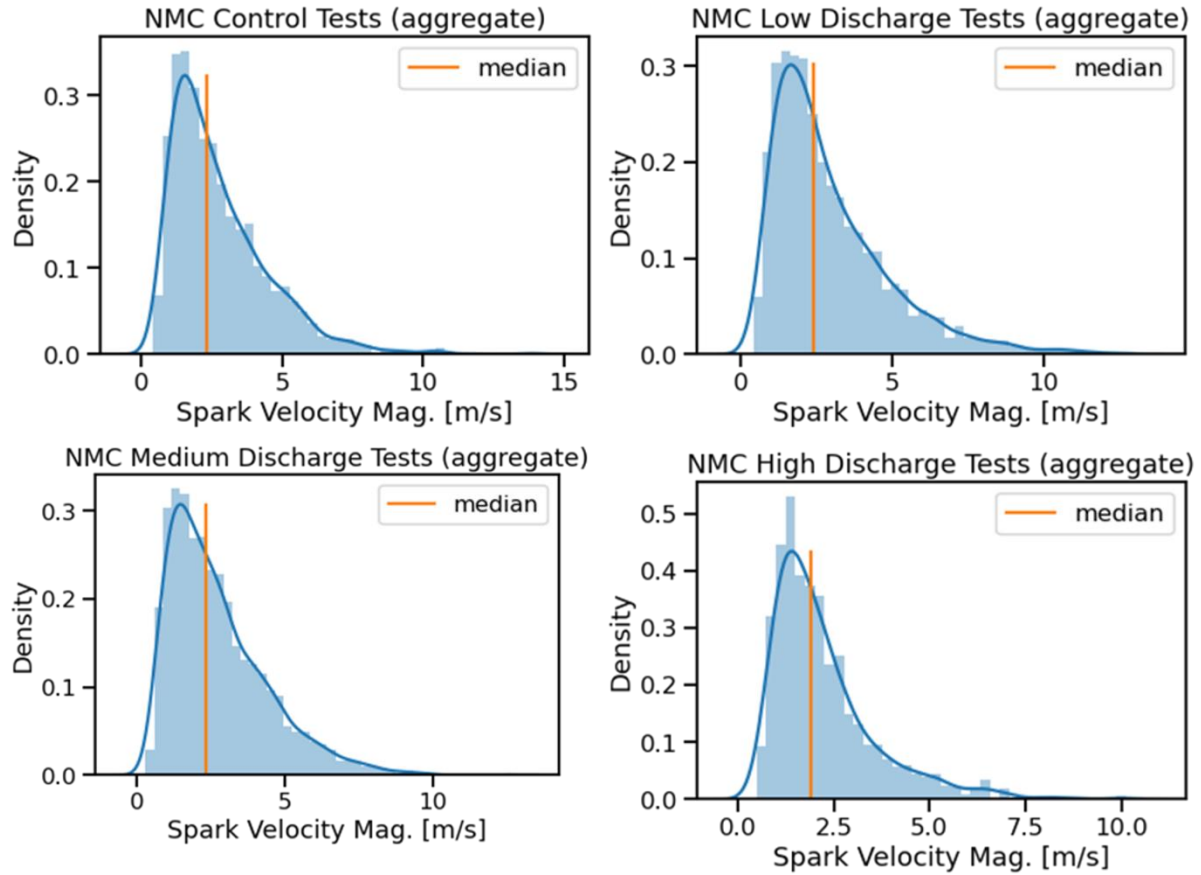


**Figure 21:** Aggregate spark velocity graphs for all NMC battery tests.

**Table 4:** Spark velocity values for NMC battery tests

	Control Tests	Low Discharge Tests	Medium Discharge Tests	High Discharge Tests
Maximum velocity (m/s)	14.0	12.8	12.56	10.13
Mean Velocity (m/s)	2.77	2.96	2.73	2.23
Median Velocity (m/s)	2.33	2.4	2.33	1.89
Minimum Velocity (m/s)	0.43	0.42	0.28	0.48

Spark velocities during the NMC battery tests were relatively consistent with the exception of the high discharge tests. Some of the high discharge NMC tests had very few sparks and their

thermal runaway reactions were much less energetic than any other test condition. This is due to the significantly lower state of charge of the NMC batteries during thermal runaway in the high-discharge tests.

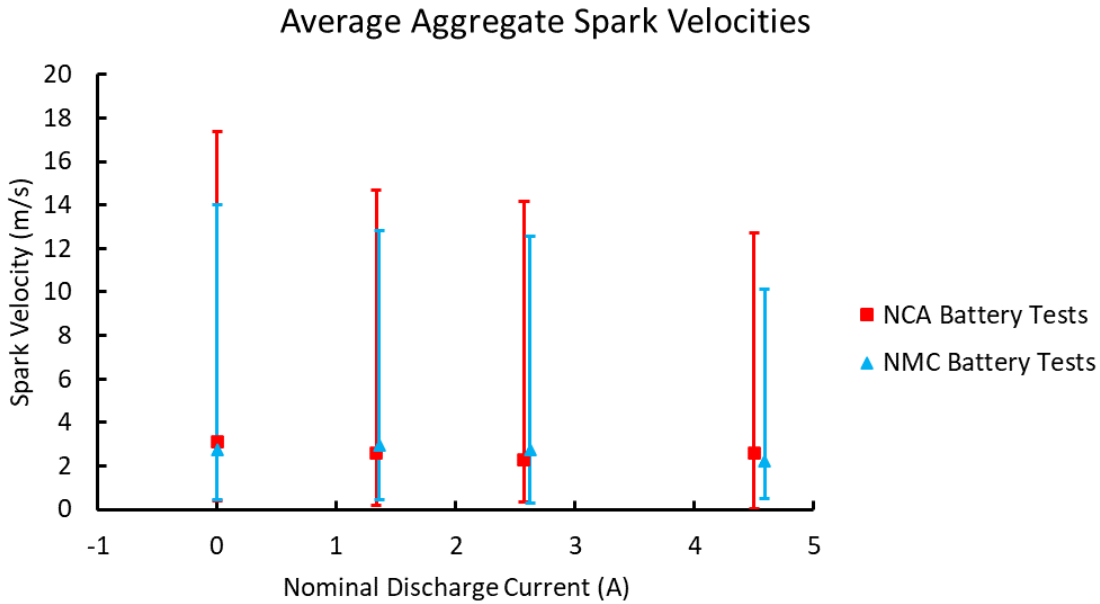


**Figure 21:** The average spark velocities of each test condition and battery type. Error bars are the maximum and minimum measured spark velocities for each test condition and battery type.

The average, maximum and minimum measured spark velocities are plotted in Figure 21. The minimum velocities do not vary significantly between test conditions and battery types, but the maximum velocities for both battery types decrease as discharge rates increase. The average spark velocity from the high discharge tests for both battery chemistries also drop from the other test conditions. Both of these patterns are likely due to the lower state of charge of the battery at thermal runaway.

## Conclusions

As lithium-ion batteries continue to be increasingly incorporated into modern technology, their safety during use and storage is a growing issue. Testing how the usage condition (discharge

current) of a lithium-ion battery impacts thermal runaway driven by thermal abuse can help ensure the worst-case scenario is accounted for when designing safety systems for lithium-ion batteries. Testing showed different results for each of the two lithium-ion battery chemistries tested. The time to thermal runaway of NCA batteries was found to decrease on average as the discharge current increased, while the time to thermal runaway for NMC batteries was found to increase if discharging was present regardless of discharge rate. Both peak internal heat generation values and maximum spark velocities decreased for both battery types as the discharge rate increased, while total internal heat generation values varied by battery type. In NMC batteries, the total internal heat generation increased as discharge current increased until the high discharge test condition, where the value dropped dramatically. While in NCA batteries almost the opposite pattern was observed, with the total internal heat generation values decreasing as discharge rate increased before rising slightly during high discharge. Testing with both battery types also saw the duration of thermal runaway increase as the discharge rate increased, though the NMC high discharge duration of thermal runaway decreased due to the lower state of charge at thermal runaway. The different responses between the battery types indicate that while the test methodology can be generalized, the behavior of lithium-ion batteries during use and thermal abuse cannot be generalized between battery chemistries.

This lack of consistency could prove to be a significant risk in a fire scenario. Those designing systems around lithium-ion batteries should consider how the specific batteries in the system would behave in a fire scenario and what safety risks they could pose. Based on this research, we believe it is important to consider battery usage (charging or discharging) in abuse scenarios and during failure. We observed that the impact of safe battery use during thermal abuse could result in different fire safety implications depending on battery chemistry and discharge current. Thus,

we believe a comprehensive testing standard should consider the impact of battery usage and how it may change depending on battery chemistry. Such a standard could be used for both existing lithium-ion battery chemistries as well as those that will be developed in the future.



## **Appendix A: Battery Test Data**

**Table A1:** Average values and 95% confidence intervals for values from NCA battery tests.

			Average Thermal Runaway Temperature (°C)	Average Safety Venting Temperature (°C)	Average Mass Loss (%)	Average Time from 55°C to Thermal Runaway (s)	Average Post-Runaway Maximum Temperature (°C)	Total Internal Heat Generation (kJ)
NCA Battery Tests	Control (0 A)	Average Value	197.17	141.20	53.12	1160.48	423.94	202.35
		95% Confidence Interval	2.38	3.56	8.58	66.37	28.45	26.29
	Low Discharge (1.33 A)	Average Value	197.8	144.58	44.39	1147.33	416.10	176.00
		95% Confidence Interval	1.69	9.56	19.642	47.55	48.72	57.83
	Medium Discharge (2.57 A)	Average Value	199.24	148.33	60.70	1115.08	361.55	152.60
		95% Confidence Interval	0.76	3.34	12.22	26.59	48.79	41.25
	High Discharge (4.50 A)	Average Value	198	148.51	56.37	1057.36	384.61	199.94
		95% Confidence Interval	1.68	4.62	12.74	17.78	69.18	39.95

**Table A2:** Average values and 95% confidence intervals for values from NMC battery tests.

			Average Thermal Runaway Temperature (°C)	Average Safety Venting Temperature (°C)	Average Mass Loss (%)	Average Time from 55°C to Thermal Runaway (s)	Average Post-Runaway Maximum Temperature (°C)	Total Internal Heat Generation (kJ)
NMC Battery Tests	Control (0 A)	Average Value	198.86	155.68	64.37	1025.28	337.08	138.06
		95% Confidence Interval	1.69	1.21	6.58	28.71	36.66	28.33
	Low Discharge (1.36 A)	Average Value	194.33	157.06	55.24	1098.04	366.27	157.22
		95% Confidence Interval	0.69	0.41	3.13	30.177	19.98	15.23
	Medium Discharge (2.62 A)	Average Value	198.86	160.80	40.91	1081.84	420.92	206.68
		95% Confidence Interval	3.22	2.24	13.15	57.98	38.95	34.35
	High Discharge (4.59 A)	Average Value	218.77	161.00	33.82	1091.28	391.60	189.38
		95% Confidence Interval	2.35	1.59	16.87	59.43	48.18	44.63

## Appendix B: Copper Slug Calorimetry Equations

Values from the calibration of the copper slug calorimeter:  $A_0, A_1, A_4, b_0, b_1, b_2, b_3, b_4$ , Cylinder mass (in grams)

Values from the test: Temperature (in Kelvin), time (in seconds), battery mass (in grams), heating power (W)

From previous research:  $C_{Battery}$

$$\text{Internal Heat Generation (W)} = Q_{Loss} + Q'_{cylinder} + Q'_{Battery} + \text{Heating Power (W)}$$

$$Q_{Loss} = \text{Heat Loss} = B * P_{Loss}$$

$$P_{Loss} = A_0 + A_1 * T + A_4 * T^4$$

$$B = \frac{b_0 + b_1 * T_x + b_2 * T_x^2 + b_3 * T_x^3 + b_4 * T_x^4}{dT/dt}$$

$$dT/dt = (T_x - T_{x-1}) / (t_x - t_{x-1})$$

$$Q'_{cylinder} = C_{cylinder} * m_{cylinder} * dT/dt$$

$$C_{cylinder} = 0.279 + (T_x^{-2} * 1.08 * 10^3) + (T_x * 4.42 * 10^{-4}) - (T_x^2 * 4.92 * 10^{-7}) \\ + (T_x^3 * 2.2 * 10^{-10})$$

$$Q'_{Battery} = C_{Battery} * m_{Battery} * dT/dt$$

## References

1. *EVENTS WITH SMOKE, FIRE, EXTREME HEAT OR EXPLOSION INVOLVING LITHIUM BATTERIES.*  
[https://www.faa.gov/hazmat/resources/lithium\\_batteries/media/Battery\\_incident\\_chart.pdf](https://www.faa.gov/hazmat/resources/lithium_batteries/media/Battery_incident_chart.pdf)  
(2020).
2. What to Know About How to Ship Lithium Batteries? *International Air Transport Association* (2021).
3. Misera, A. M. & Long, R. T. Sprinkler Protection Guidance for Lithium-Ion Based Energy Storage Systems. *NFPA Research Foundation* (2019).
4. Wang, Q., Mao, B., Stoliarov, S. I. & Sun, J. A review of lithium ion battery failure mechanisms and fire prevention strategies. *Progress in Energy and Combustion Science* (2019) doi:10.1016/j.pecs.2019.03.002.
5. Wagner, R., Preschitschek, N., Passerini, S., Leker, J. & Winter, M. Current research trends and prospects among the various materials and designs used in lithium-based batteries. *Journal of Applied Electrochemistry* vol. 43 (2013).
6. BU-205: Types of Lithium-ion. *Battery University* (2021).
7. Kim, J. H., Lee, K. H., Ko, D. C., Lee, S. B. & Kim, B. M. Design of integrated safety vent in prismatic lithium-ion battery. *J. Mech. Sci. Technol.* **31**, (2017).
8. Battery Guy. Safety issues with lithium batteries. (2019).
9. Keep Your Batteries Safe. *batteryjunction.com*.
10. Tanim, T. R., Garg, M. & Rahn, C. D. An intelligent nail design for lithium ion battery penetration test. in *ASME 2016 10th International Conference on Energy Sustainability, ES 2016, collocated with the ASME 2016 Power Conference and the ASME 2016 14th International Conference on Fuel Cell Science, Engineering and Technology* vol. 2 (2016).
11. Yamanaka, T., Takagishi, Y., Tozuka, Y. & Yamaue, T. Modeling lithium ion battery nail penetration tests and quantitative evaluation of the degree of combustion risk. *J. Power Sources* **416**, (2019).
12. Zhao, R., Liu, J. & Gu, J. Simulation and experimental study on lithium ion battery short circuit. *Appl. Energy* **173**, (2016).
13. Fu, Y., Lu, S., Shi, L., Cheng, X. & Zhang, H. Ignition and combustion characteristics of lithium ion batteries under low atmospheric pressure. *Energy* (2018)  
doi:10.1016/j.energy.2018.06.129.
14. Guo, F. *et al.* Experimental study on flammability limits of electrolyte solvents in lithium-ion batteries using a wick combustion method. *Exp. Therm. Fluid Sci.* **109**, (2019).
15. Barkholtz, H. M. *et al.* Multi-scale thermal stability study of commercial lithium-ion batteries as a function of cathode chemistry and state-of-charge. *J. Power Sources* (2019)

doi:10.1016/j.jpowsour.2019.226777.

16. Larsson, F., Andersson, P., Blomqvist, P. & Mellander, B. E. Toxic fluoride gas emissions from lithium-ion battery fires. *Sci. Rep.* **7**, (2017).
17. Jian Hu, Tong Liu, Xishi Wang, Zhigang Wang & Liusuo Wu. Investigation on thermal runaway of 18,650 lithium ion battery under thermal abuse coupled with charging. *J. Energy Storage* **51**, (2022).
18. Plunkett, S. T. *et al.* Enhancing thermal safety in lithium-ion battery packs through parallel cell ‘current dumping’ mitigation. *Appl. Energy* **286**, (2021).
19. Quintiere, J. G. On methods to measure the energetics of a lithium ion battery in thermal runaway. *Fire Saf. J.* **111**, (2020).
20. PRODUCT SPECIFICATION Rechargeable Lithium Ion Battery Model : INR18650 MH1 3200mAh. *LG Chem* (2014).
21. NCR18650A Datasheet (PDF) - Panasonic Battery Group. *Panasonic Battery Group* (2012).
22. Superwool Board Data Sheet.
23. Lutum, R., Heck, S. & Scheuerlein, C. Electrical resistance of the solder connections for the consolidation of the LHC main interconnection splices. *IEEE Trans. Appl. Supercond.* **23**, (2013).
24. Liu, X., Stoliarov, S. I., Denlinger, M., Masias, A. & Snyder, K. Comprehensive calorimetry of the thermally-induced failure of a lithium ion battery. *J. Power Sources* (2015) doi:10.1016/j.jpowsour.2015.01.125.